# Graphene Oxide-Coated Gold Nanorods

Subjects: Nanoscience & Nanotechnology

Contributor: Thabang C. Lebepe , Sundararajan Parani , Oluwatobi S. Oluwafemi

The application of gold nanorods (AuNRs) and graphene oxide (GO) has been widely studied due to their unique properties. Although each material has its own challenges, their combination produces an exceptional material for many applications such as sensor, therapeutics, and many others

gold nanorods graphene oxide photothermal sensors Theranostic

## 1. Introduction

AuNRs are described as particles with an aspect ratio between 2 and 25. AuNRs are single-crystalline, which orient in either the {100} or {111} or {110} directions, as shown in transmission electron microscopy images[1] [14]. AuNRs produce the longitudinal surface plasmon resonance (LSPR) and transverse surface plasmon resonance (TSPR) in the absorption spectroscopy[1][2][3]. TSPR occurs due to the oscillation of free surface electrons along the width of the rod, which is usually observed in the visible region around λabs = 510–530 nm. TSPR show a little dependence on the aspect ratio of AuNRs. On the contrary, LSPR occurs due to oscillation along the length of the rod and is observed in the near-infrared (NIR) region. LSPR strongly depends on the AR. The higher the aspect ratio, the longer the absorption wavelength. AuNRs are also highly sensitive to local environmental changes, making them excellent materials for many applications[4]. Biomedical applications of AuNRs focus mainly on their potential to deliver/control release drugs and their therapeutic action against cancer, bacteria, and viruses[5][6]. In addition, AuNRs have also been used in other fields such as optical power limiters, solar cells, light-emitting diodes, stress/strain sensors, and catalysis[7][8].Graphene oxide (GO) is a single atomic layer thick two-dimensional material, which is a derivative of graphene with various oxygen-containing functionalities such as epoxides, hydroxyl groups, and carboxyl groups[9]. Unlike hydrophobic graphene, GO is hydrophilic due to the oxygen functionalities and hence, it is soluble in water[10]. GO has a honeycomb carbon structure with many defects localized inside as well as over the surface planes and edges induced by oxidation[11]. The structural properties of GO make it an ideal material of choice in the field of biomedicine, especially theranostic, due to its solubility in aqueous mediums, better colloidal stability, cost-effectiveness, scalability, and large surface area (≈2630 m2/g) and thermal property mostly in the reduced form[12][13][14]. GO has an exceptional capability to immobilize a huge quantity of substances, including metals, drugs, biomolecules, and fluorescent probes and cells[15]. Moreover, it has been reported to have intrinsic and NIR absorbance properties, which make it useful as a photothermal agent for cancer treatment[9][13][14][16]. The combination of GO and AuNRs (GO–AuNRs) advances the applications of this composite material in theranostic[17][18][19][20][21][22][23][24], biocarrier[18][24], imaging[20][25][26][27], and also sensors[28][29][30][31][32][33]. The properties and application of GO–AuNRs composites are discussed below.

## 2. Biocompatibility

The biocompatibility of all nanomaterials is very essential, especially if the materials are to be used for biological application. Numerous studies on nanomaterials' cytotoxicity have shown that the size, surface charge, and capping agents are mostly responsible for the toxicity found in nanomaterials[34][35][36][37]. AuNRs are mostly synthesized with CTAB as a surfactant, which causes the toxicity of the material[6][38]. In contrast, GO has been shown to be biocompatible, and the combination of AuNRs and GO has been shown to produce a more biocompatible composite compared to unmodified AuNRs. In a recent development, Qiu et al.[25] evaluated the cytotoxicity of GO@AuNRs against adenocarcinomic human alveolar basal epithelial cells (A549 cells) (Figure 1a). They observed that GO@AuNRs were more biocompatible even at 200 μM than bare AuNRs[25]. In another study, gold nanorod-decorated (AuNRs–PEG–GO) nanocomposites were reported to be biocompatible when their cytotoxicity was evaluated against epidermoid carcinoma cells (A431 cells). Cellular internalization from dark-field microscopy, confocal Raman microscopy, and transmission electron microscopy (TEM) confirmed that AuNRs–PEG–GO did not affect concentrations up to 1 ppm (Figure 1b–c)[17].

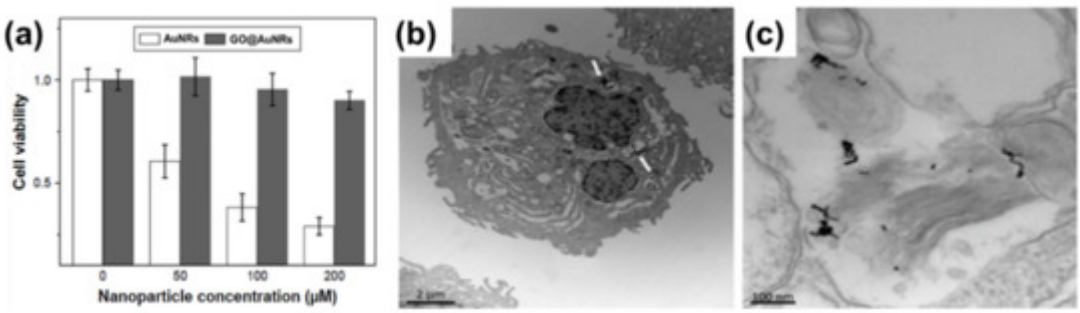


**Figure 1.** (**a**) Cell viabilities of AuNRs and GO@AuNRs against A549 cells. Reproduced from[25], with permission from Dove Medical Press, 2017. (**b**,**c**) High-magnification transmission electron microscopy image of internalization of AuNRs–PEG–GO composite in a cells. Adapted from[17], with permission from Wiley, 2013.

Lim et al.[18] reported the synthesis of plasmonic gold nanoshells (AuNSs) and AuNRs coated with rGO and evaluated their cytotoxicity against human umbilical vein endothelial cells (HUVECs). HUVECs exposed to GO-coated particles for 24 h at an optical density of 1.0 had no significant cytotoxicity[18]. Another study by Sun et al.[26] reported the cell viability of the human pancreatic adenocarcinoma cell line (SW1990 cancer cells) against GO–PSS–AuNRs (Figure 2a). Different concentrations of GO–PSS–AuNRs nanohybrids (0–200 μg/mL) exposed to the cells for 24 h were measured by a Cell Counting Kit-8 (CCK-8) assay, and all concentration tested showed no significant toxicity, even at high concentration (200 μg/mL). The in vivo long-term toxicity assessment of the GO–AuNRs after a month of exposure did not show obvious inflammation, cell necrosis, or apoptosis to normal organs (Figure 2b)[26].

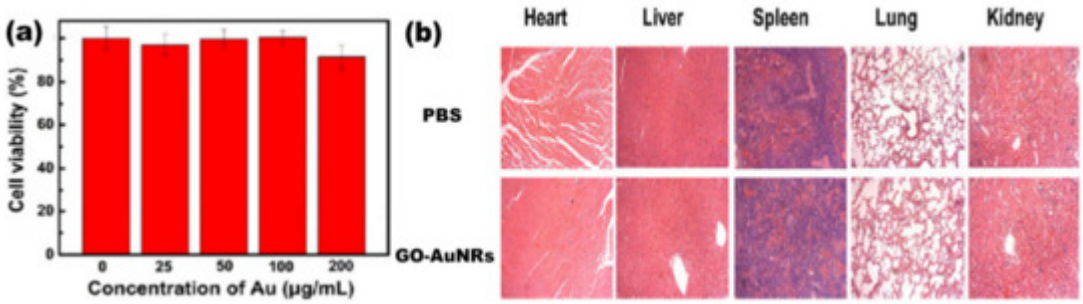


**Figure 2.** (**a**) Cytotoxicity of GO–PSS–AuNRs solutions with various Au concentrations against SW1990 cancer cells. (**b**) Histological images of the heart, liver, spleen, lung, and kidney of the mice, obtained one month after intravenous injection with phosphate buffer solution (PBS, 100 μL) and GO–AuNRs (0.026 M, 100 μL). Adapted from[26], with permission from Springer Nature, 2016.

## 3. Photothermal Properties

The photothermal properties of AuNRs and GO have been researched widely as individual entities and both AuNRs and GO have shown remarkable in vitro and in vivo photothermal efficiency[17][18][22][23][26][39][40][41][42]. However, GO needs to be reduced to have these properties, because GO has a highly oxidized structure with a disrupted π conjugation, which lowers its conductivity[18][21]. The photothermal property of AuNRs is due to its surface plasmonic resonance, and as mentioned earlier, AuNRs have two types of surface plasmonic resonance peaks[43][44][45][46][47][48]. Numerous studies have shown that AuNRs can generate much heat when exposed to a specific laser with a wavelength corresponding to its LSPR[43][49][50]. The combination of AuNRs and GO for effective photothermal properties has been studied[17][18][19][20][22][23][24][27][42]. Dembereldor et al.[17] investigated the photothermal effect of the AuNRs–PEG–GO nanocomposites against A431 cells. The AuNRs–PEG–GO was found to produce heat when exposed to a laser with a 60 W/cm$^2$ for 5 min. This nanocomposite was able to significantly destroy the cells by ≈40% when irradiated with light.[17]. Lim and co-workers [19] reported a comparative study of AuNRs and gold nanoshells (AuNSs) coated with rGO. rGO–AuNRs showed outstanding photothermal property compared to the uncoated AuNRs, AuNSs, and rGO–AuNSs[19]. Sun et al.[26] reported that the GO–PSS–AuNRs displayed an outstanding photothermal effect in vitro (Figure 3a). The temperature of the GO–PSS–AuNRs nanohybrids increased from 25 to 49.9 °C at a concentration of 50 μg/mL after irradiation with an 808-nm laser (0.4 W/cm$^2$) for 6 min (Figure 3b). In addition, GO–PSS–AuNRs exhibited good optical and morphological stability and photothermal properties, even after six cycles of laser irradiation[26]. Khan et al. [18] prepared GO@AuNRs by functionalizing natural polymer gum arabic to reduce GO, which was further conjugated to AuNRs to increase its photothermal profiling. An infrared camera was able to detect up to 59.3 ℃ heat produced by GO–AuNRs (Figure 3c)[18]. In another development, Turcheniuk et al.[23] investigated the potential of PEG-functionalized rGO–PEG enrobed AuNRs conjugated to Tat protein for the photothermal destruction of human glioblastoma astrocytoma (U87MG) cells in mice. The Tat protein was used to make the composite target selective. In vivo studies showed that the composite was able to suppress U87MG tumor growth in mice[23].

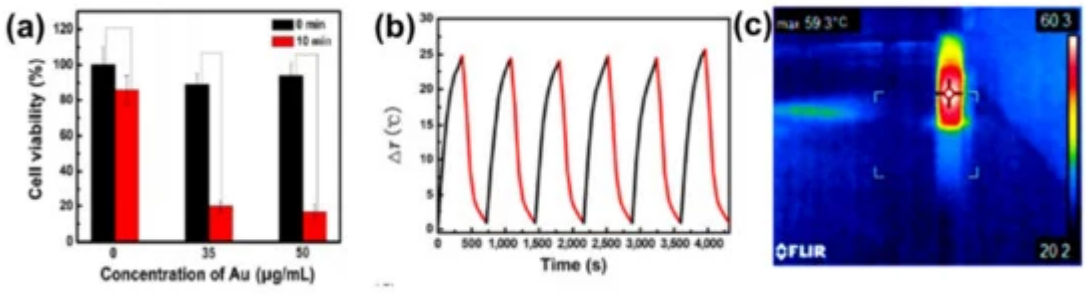


**Figure 3.** (**a**) Phototoxicity assay of SW1990 cells in the presence of different amounts of GO–PSS–AuNRs with or without laser irradiation (808 nm) for 10 min. (**b**) Photothermal profiling of on and off cycle of GO–AuNRs (50 μg/mL) for 4000 s. Adapted from[26], with permission from Springer Nature, 2016. (**c**) IR image of GO–AuNRs irradiated with laser. Adapted from[18] with permission from Elsevier, 2017.

# 4. Applications

## 4.1. Biomedical Application: Theranostic Agent

The combination of therapy and diagnosis that is also known as theranostic is becoming one of the most interesting studies in cancer research[51] due to its great potential in personalized cancer medicine. The theranostic agent must have a characteristic such as the ability to diagnose a disease, its status, and its response to a specific treatment while at the same time perform treatment[52]. The coating of AuNRs with GO has produced a material that is biocompatible and useful in biomedical application. However, studies of GO-coated AuNRs as a theranostic agent are still rare in cancer therapy. The most common studies of GO–AuNRs are based on conjugation with a cancer drug. Song et al.[22] fabricated an rGO–AuNRs vesicle (Ve) with remarkably amplified photoacoustic (PA) performance and photothermal effects when loaded with doxorubicin (DOX). Both the cavity of the vesicle and the large surface area of the encapsulated rGO can be used for loading DOX, making it an excellent drug carrier. The combination of chemo- and photothermal therapies revealed an effective inhibition of tumors. The in vivo studies of rGO–AuNRsVe–DOX generated more heat even at low power density than bare rGO–AuNRsVe (Figure 4a). The tumor-bearing mice were intravenously injected with PBS, DOX, and rGO–AuNRsVe–DOX and exposed to the 808 nm laser at different power densities (Figure 4b). The relative tumor volume was reduced when treated with rGO–AuNRsVe–DOX irradiated at lower power density compared with bare rGO–AuNRsVe irradiated at higher power density. The tumor tissue section under treatment with rGO–AuNRsVe–DOX irradiated with laser showed more severe cancer necrosis and fewer cancer cells (Figure 4c). On the contrary, mice treated with PBS, laser irradiation, or rGO–AuNRsVe–DOX without laser irradiation did not exhibit any tumor necrosis[22].

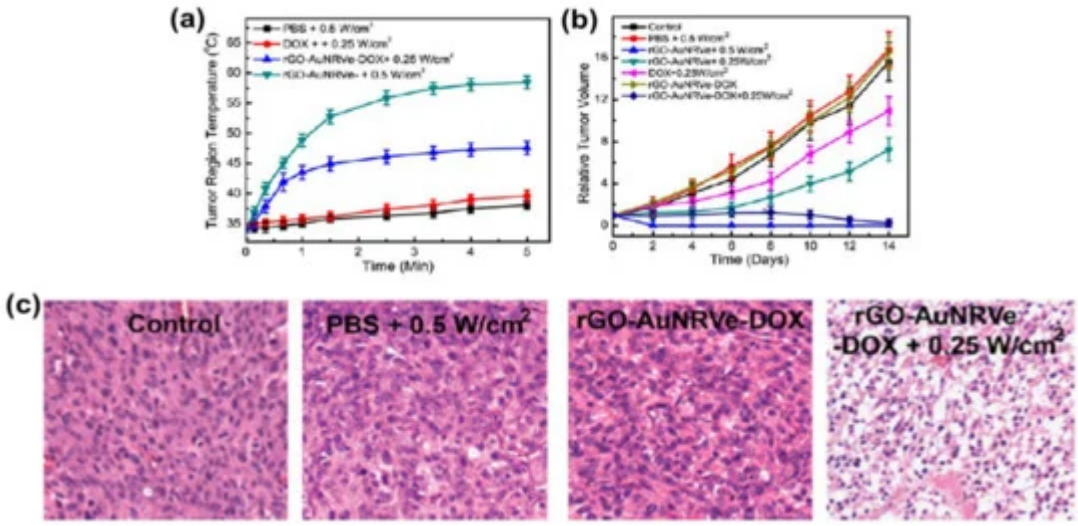


**Figure 4.** (**a**) Tumor region temperature changes of the mice treated with PBS, DOX, and rGO–AuNRsVe–DOX irradiated with an 808 nm laser of different power densities for 5 min. (**b**) Relative tumor volume of the tumor-bearing mice after intravenous injection of the samples and exposed to the 808 nm laser at different power densities. Tumor volumes were normalized to their initial sizes. (**c**) Images of H&E (hematoxylin and eosin)-stained tumor sections harvested from the tumor-bearing mice treated with PBS and rGO–AuNRsVe–DOX with or without laser irradiation. Adapted from[22] with permission from American Chemical Society, 2015. Ve: vesicle.

Khan et al.[18] also reported DOX conjugated to GO–AuNRs, however, with a little modification whereby GO was first functionalized with GA before coating with AuNRs and conjugation with DOX. The drug release kinetics under physiological conditions using standard statistical models demonstrated that at pH 5.8, 82% of DOX from GO–AuNRs–DOX was released under laser irradiation (Figure 5a). GO–AuNRs were shown to have low dark toxicity in both Hela and A549 cells; however, when conjugated to DOX, a significant decrease in cell viability occurred, and there was even more when the laser was applied (Figure 5b). The in vivo experiment results indicated that when mice were treated by only DOX, it caused liver and kidney tissue damage (Figure 5c). In contrast to DOX, the GO–AuNRs–DOX showed no damage to the organs. The tissue damage by DOX alone was believed to be due to the high uptake of the drug; however, the biocompatibility of GA used on the complex and slow release of DOX was reported to be the reason, while no organ was damaged, even after irradiation.[18].

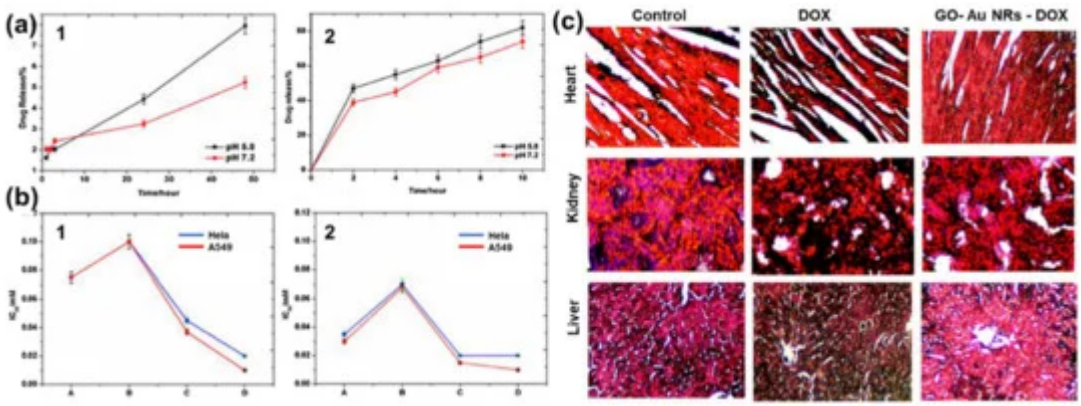

**Figure 5.** (**a**) Percentage of drug release with respect to time (**1**) without near-infrared (NIR) and (**2**) with NIR irradiation. (**b**) $IC_{50}$ values on in vitro cell lines (**1**) without NIR irradiation and (**2**) with NIR irradiation**.** (**c**) Histological images of a heart, kidney, and liver treated by DOX and fGO–AuNR–DOX Adapted from[18] [30], with permission from Elsevier, 2017.

Xu et al.[24] demonstrated that AuNRs encapsulated in GO decreased the toxicity of the surfactant-coated AuNRs and offered high surface area for the conjugation of hyaluronic acid. The composite was used to load DOX, which was demonstrated to be more effective than chemo- and photothermal therapy when used separately[24]. Zang et al.[27] introduced mesoporous silica on an rGO–AuNRs composite ($Au/SiO_2$/rGO) and also conjugated it to DOX. $Au/SiO_2$/rGO nanohybrids exhibited photothermal stability and good drug release.[27]. Qi et al. recently reported the immobilization of AuNRs onto the surface of GO–PEG via polydopamine (PDA) to fabricate AuNRs/GO@PDA hybrid nanosheets. The AuNRs/GO@PDA hybrid nanosheets were photostable and biocompatible with a photothermal conversion efficiency of 14.1%, which was higher than the bare AuNRs. In addition, AuNRs/GO@PDA was an efficient drug carrier that possessed a loading ability for DOX of up to 86.16%[53]. More studies using GO-coated AuNRs still need to be conducted to advance its usefulness as a theranostic agent.

## 4.2. Sensors

The application of GO–AuNRs as an analytical sensor has gained more interest due to their unique properties of both AuNRs and GO. The surface plasmon resonance (SPR) of AuNRs is one of the reasons why it has emerged as an excellent tool for sensing applications[54], while the GO with various oxygen functional groups can also act as a molecular sensor[55]. The integration of AuNRs-decorated GO have been shown to enhance the sensing performance[56][28][29][32][33][57][58][59][60]. Both of these materials have been used for various applications from biosensors to chemosensors, for the detection of DNA, pollutants, diseases, and drugs, to mention a few. Fu et al.[31] developed GO–AuNRs for the detection of heparin by applying the color-quenching capacity of GO. Briefly, AuNRs were self-assembled onto the surface of GO through electrostatic interaction (Figure 6a), which decreased the LSPR as well as its appearance. The original color was restored by adding polycationic protamine due to its strong interaction with GO and its strong affinity for heparin over GO. The sensor experiments were carried out in a 4- (2-Hydroxyethyl)-1-piperazineethanesulfonic acid buffer (pH 7.4, 10 mM) at room temperature. The result showed a linear relationship to heparin concentration, ranging from 0.02 to 0.28 μg/mL (R = 0.9957) with a detection limit of 5 ng/mL (Figure 6b). Figure 6c shows the photographic images of the corresponding colorimetric responses with the increase of heparin concentration[31].

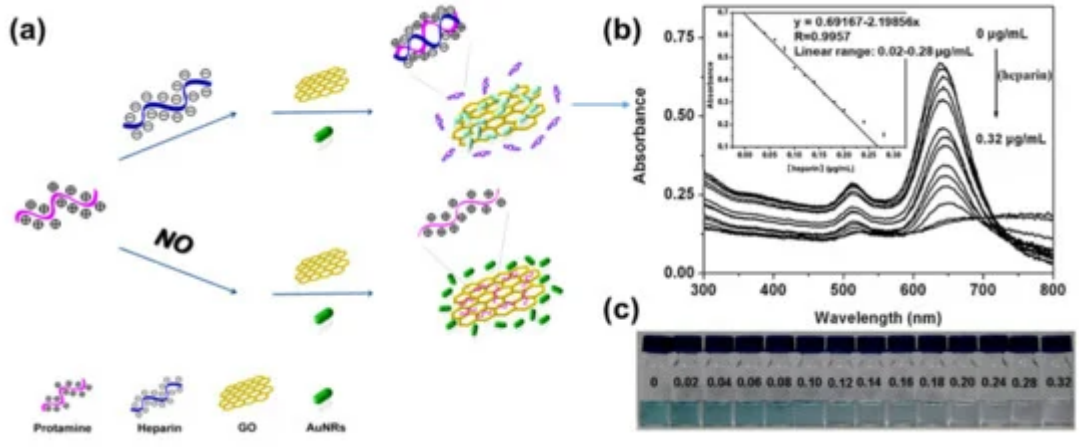


**Figure 6.** (**a**) Schematic of GO–AuNRs protamine mixed sensor for detecting heparin. (**b**) Absorption spectra of GO–AuNRs protamine mixed solution with difference heparin concentrations. Inset: heparin detection calibration curve (**c**) Photographic images of the corresponding colorimetric responses with the increase of heparin concentration. Adapted from[31], with permission from Elsevier, 2012.

In another development, Zhang and co-workers[61] reported an SPR-based biosensor for the detection of transferrin using GO decorated with AuNRs–antibody conjugates carried out in a reactor using phosphate buffer solution (PBS) as the baseline solution. In this study, AuNRs were anchored on the surface of GO with the antibody (rabbit anti-transferrin), which served as an enhancer for the detection of transferrin. The AuNRs–GO antibody conjugate biosensor showed a detection response to transferrin in the concentration range of 0.0375–40 μg/mL[61]. Deng et al.[58] also reported the coating of a glassy carbon electrode (GCE) with AuNRs-decorated GO nanosheets. The AuNRs facilitated the electrochemical reduction of GO. The electrochemically reduced graphene oxide decorated with AuNRs demonstrated high accumulation efficiency and considerable surface enhancement effects for the electro-oxidation of sunset yellow and tartrazine. The probe had a linear response to sunset yellow and tartrazine in the concentration range of 0.01–3.0 μM and 0.03–6.0 μM with detection limits of 2.4 and 8.6 nM, respectively[58]. Arvand and Gholizadeh[28] investigated an AuNRs–GO nanocomposite incorporated carbon nanotube paste-modified glassy carbon electrode. The square wave voltammetry electrochemical method was used for the determination of indomethacin in aqueous media (PBS, pH 8.0). This probe demonstrated a high effective surface area, more reactive sites, and excellent electrochemical catalytic activity toward the oxidation of indomethacin with two linear calibration ranges of 0.2–0.9 and 2.5–91.5 μM and exhibited an excellent limit of detection of $1.7 \times 10^{-2}$ μM. The sensor was further used to detect indomethacin in pharmaceutical samples (tablet and capsules), human blood serum, and urine obtained from the patients who underwent treatment with indomethacin. The accuracy of determination was not different from the labeled values on the pharmaceutical samples by more than 2.56%. The recovery of indomethacin from the blood and urine was reported to be from 98.0% to 103.5%, respectively[28].

AuNRs-decorated GO sheets have also been used as a simple electrochemical sensor for sensitive and selective DNA detection. Differential pulse voltammetry (DPV) was used to monitor the DNA hybridization occurrence with methylene blue as an electrochemical indicator. The methylene blue peak currents were linear with the logarithm of

the concentrations of complementary DNA from $1.0 \times 10^{-9}$ to $1.0 \times 10^{-14}$ M, and the detection limit of the probe was measured to be $3.5 \times 10^{-15}$ M. Furthermore, this electrochemical sensor probe can distinguish complementary DNA sequences in the presence of a large amount of single-base mismatched DNA (1000:1), indicating that the biosensor has high selectivity[32]. Similarly, an electrochemical biosensor for the detection of specific-sequence target DNA has been reported by Shi et al.[60]. The biosensor was fabricated based on a "sandwich-type" detection strategy, which involved a capture probe immobilized on the surface of the AuNRs-decorated rGO sheets, gold nanoparticles as a reporter probe to flank the target DNA, and adriamycin. Adriamycin was used as an electrochemical indicator because of its ability to electrostatically bond with anionic phosphate of DNA strands. The peak currents of adriamycin in DPV were linear with the logarithm of target DNA concentration in the range of $1.0 \times 10^{-16}$ to $1.0 \times 10^{-9}$ M. The probe had a detection limit of $3.5 \times 10^{-17}$ M. This sandwich-type sensor exhibited good selectivity, even for single-base mismatched target DNA detection. In another study by Azimzadeh et al.[29], GCE modified with a thiolated probe-functionalized AuNRs-decorated GO sheet was used to detect a different nucleic acid (miRNA), using oracet blue as an indicator in a DPV. In addition, AuNRs–GO exhibited high specificity, with the ability to differentiate between complementary target miRNA, single-, three-base mismatch, and non-complementary miRNA. The GCE modified with thiolated-functionalized GO–AuNRs has an electrochemical signal (peak current) linear relationship with the concentration of the target miRNA ranging from 2.0 fM to 8.0 pM and a detection limit of 0.6 fM. All electrochemical sensing was carried out in a phosphate buffer solution (pH 7.0)[29]. Cao et al.[30] constructed GO–AuNRs multi-labeled with glucose oxidase (GOD) and streptavidin (SA) to form a luminol-based electrochemiluminescence (ECL) aptasensor for detecting prostate-specific antigen (PSA) (Figure 7a). To achieve multiple signal amplification, GOD and SA–biotin–DNA were deposited on GO–AuNRs to form a signal probe. The addition of glucose produced $H_2O_2$ due to the catalytic effect of GOD incorporated on the probe, while the AuNRs reacted with the $H_2O_2$ to produce reactive oxygen species in a luminol ECL reaction. The combination of SA with biotin–DNA was used to intensify the ECL signal intensity. The addition of PSA interfered with the interaction between signal amplifiers and the electrode by attaching to PSA aptamers to block/cleave the signal amplifiers, which caused the loss of the ECL signal, as shown in Figure 7b. This ECL biosensor had a linear range of 0.5 pg/mL to 5.0 ng/mL with the detection limit of 0.17 pg/mL (S/N = 3). The ECL biosensor was further used to detect PSA in human serum samples; the recoveries were between 81.4% and 116.0%, with a relative standard deviation varying from 2.8% to 10.2%[30].

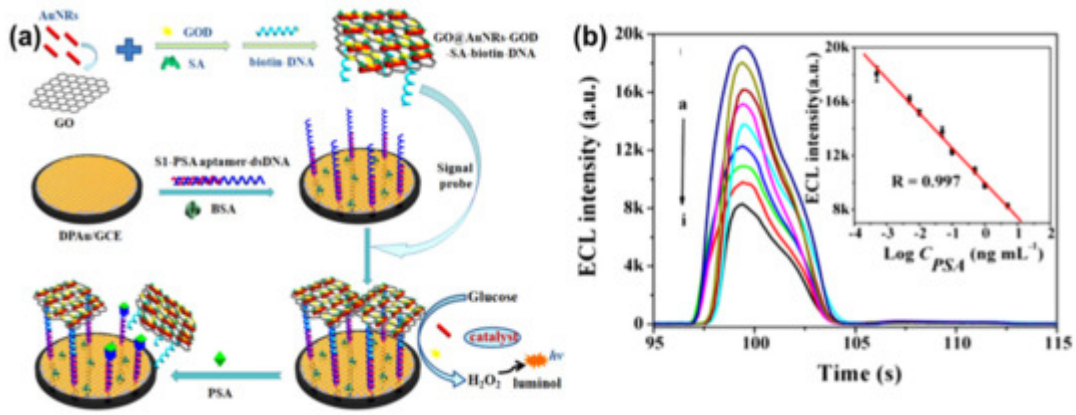

**Figure 7.** (**a**) Schematic diagram of GO–AuNRs multi-labeled with glucose oxidase and streptavidin toward luminol-based electrochemiluminescence (ECL) aptasensor for prostate-specific antigen detection. (**b**) Electrochemiluminescence intensity changes with prostate-specific antigen (PSA) concentrations (ng/mL), insert: The detection of prostate-specific antigen calibration curve. Adapted from[30], with permission from Elsevier, 2018.

Another ECL aptasensor based on a dual-potential signal amplification strategy triggered by graphene/hemin/gold nanorods/G-quadruplex–hemin (rGO–H–AuNRs–G4H) composite was reported by Govindaraju et al.[62]. The rGO–H–AuNRs–G4H showed a good linear detection of thrombin ranging from 100 ng/mL to 0.5 pg/mL linearly, with a detection limit of 4.2 fg/mL[63]. Jayabal et al. [33] reported reduced graphene oxide–AuNRs embedded in an amine-functionalized silicate sol–gel matrix (rGO–Au–TPDT NRs) composite for the electrochemical sensing of nitric oxide (NO). The mechanism of this probe was based on the oxidation of NO by the synergistic catalytic effect of the composite material. The amperometric current of this probe exhibited a linear relationship with the NO concentration ranging from 10 to 140 nM. The probe had a detection limit of ≈6.5 nM. Nirala et al.[59] proposed a bioelectrode from partially reduced GO–AuNRs reinforced with chitosan fabricated on Indium Tin Oxide (CH–prGO–AuNRs/ITO) for glucose detection. These CH–prGO–AuNRs/ITO bioelectrodes showed a high sensitivity of current 3.2 μA/(mg/dL)/cm$^2$. CH–prGO–AuNRs exhibited a linear range of 25–200 mg/dL with a low detection limit of 14.5 mg/dL. Furthermore, these CH–prGO–AuNRs/ITO-based electrodes demonstrated synergistically enhanced sensing properties when compared to simple graphene oxide-based CH–GO/ITO electrode. Liu et al.[64] presented a different approach by applying the surface-enhanced Raman spectroscopy (SERS) method with GO–AuNRs as a probe for the detection of hepatitis B surface antigen (HBsAg). This biosensor showed a SERS signal that increased as the HBsAg concentration increased from 1 to 1000 pg/mL with a detection limit of 50 × 10$^{-3}$ pg/mL. They further used the sensor probe to detect hepatitis B in human blood samples from nine infected patients, the detection relative standard deviation was less than ±5%, and the recovery was 96–104%[64]. Lu et al. [65] reported a different approach, where bovine serum albumin-coated silver indium sulfide quantum dots (BSA-AIS) were used as photoelectrochemical (PEC) sensors fabricated with AuNRs and GO for the detection of dopamine (DA). GO and AuNRs were used to enhance the catalytic and photoelectric properties of the sensors. The BSA-AIS/AuNRs/GO-based PEC probe showed sensitivity in the linear range of 0.3–10 μM and detection limit of 66.8 nM. The same probe was shown to be selective for DA detection over the interfering substances of ascorbic acid and uric acid[65].

## 4.3. Other Applications

GO–AuNRs have also been applied in antibacterial, photoacoustic, and SERS bioimaging application. Turcheniuk and co-workers developed non-antibiotic-based treatments against bacterial infections by Gram-negative apathogenic. Their report illustrated that AuNRs coated with rGO–PEG (rGO–PEG–AuNRs) functionalized with multimeric heptyl α-D-mannoside can selectively kill uropathogenic Escherichia coli UTI89 bacteria causing urinary infection[42]. In another work, Moon et al. reported the photoacoustic (PA) performance of rGO–AuNRs. Simulation results revealed that rGO–AuNRs can generate a higher magnitude of the enhanced electromagnetic field, which is a promising deep-tissue imaging probe due to remarkably high PA amplitudes[20]. Qiu et al. investigated GO–AuNRs for ultrafast NIR SERS bioimaging. The GO–AuNRs in vitro study indicated that it had a higher NIR SERS

activity in comparison to traditional gold nanostructures. Hence, it can be a promising probe for NIR SERS-based bioimaging applications[25].

## 5. Conclusions, Remarks, and Future Prospects

In conclusion, the application of GO–AuNRs composites is growing continuously. The cytotoxicity of GO–AuNRs were discussed, which revealed the biocompatibility of GO–AuNRs composite in both cell and animal studies. The photothermal properties of GO–AuNRs from different reports showed that GO is not only making AuNRs biocompatible but also increasing its photothermal properties. Furthermore, different applications of GO–AuNRs in photothermal therapy, theranostics, sensors, as an antibacterial agent, photoacoustic, and SERS bioimaging were also discussed. Although AuNRs–GO composites have been useful for many applications, some issues such as the weak interaction of AuNRs with GO, which leads to the aggregation and the non-uniform distribution of AuNRs on the GO sheet, still need to be addressed. In addition, the biological application of GO–AuNRs still needs further investigation. The toxicity of this composite needs to be deeply understood by studying the mechanism of interaction between the cell and the composite, as well as the cellular uptake. Furthermore, the biosensor of this composite needs to be investigated more in real samples.

## References


1. Xiaoshan Kou; Shuzhuo Zhang; Chia-Kuang Tsung; Zhi Yang; Man Hau Yeung; Galen D. Stucky; Lingdong Sun; Jianfang Wang; Chunhua Yan; One-Step Synthesis of Large-Aspect-Ratio Single-Crystalline Gold Nanorods by Using CTPAB and CTBAB Surfactants. *Chemistry - A European Journal* **2007**, *13*, 2929-2936, 10.1002/chem.200601224.
2. Liu, X.; Yao, J.; Luo, J.; Duan, X.; Yao, Y.; Liu, T. Effect of Growth Temperature on Tailoring the Size and Aspect Ratio of Gold Nanorods. Langmuir 2017, 33, 7479–7485.
3. Pérez-Juste, J.; Pastoriza-Santos, I.; Liz-Marzán, L.M.; Mulvaney, P. Gold nanorods: Synthesis, characterization and applications. Coord. Chem. Rev. 2005, 249, 1870–1901.
4. Nthabeleng Hlapisi; Tshwafo Elias Motaung; Linda Z. Linganiso; Oluwatobi S. Oluwafemi; Sandile P. Songca; Encapsulation of Gold Nanorods with Porphyrins for the Potential Treatment of Cancer and Bacterial Diseases: A Critical Review.. *Bioinorganic Chemistry and Applications* **2019**, *2019*, 7147128, 10.1155/2019/7147128.
5. Laura C. Kennedy; Lissett R. Bickford; Nastassja A. Lewinski; Andrew J. Coughlin; Ying Hu; Emily S. Day; Jennifer L. West; Rebekah Anna Drezek; A New Era for Cancer Treatment: Gold-Nanoparticle-Mediated Thermal Therapies. *Small* **2010**, *7*, 169-183, 10.1002/smll.201000134.
6. Joshua M. Allen; Junpeng Xu; Maria Blahove; Stephanie A. Canonico-May; Taylor J. Santaloci; Martha E. Braselton; John Stone; Synthesis of less toxic gold nanorods by using

dodecylethyldimethylammonium bromide as an alternative growth-directing surfactant. *Journal of Colloid and Interface Science* **2017**, *505*, 1172-1176, 10.1016/j.jcis.2017.06.101.

7. Rasha N. Moussawi; Digambara Patra; Synthesis of Au Nanorods through Prereduction with Curcumin: Preferential Enhancement of Au Nanorod Formation Prepared from CTAB-Capped over Citrate-Capped Au Seeds. *The Journal of Physical Chemistry C* **2015**, *119*, 19458-19468, 10.1021/acs.jpcc.5b04447.
8. Nathan D. Burrows; Samantha Harvey; Fred A. Idesis; Catherine J. Murphy; Understanding the Seed-Mediated Growth of Gold Nanorods through a Fractional Factorial Design of Experiments. *Langmuir* **2016**, *33*, 1891-1907, 10.1021/acs.langmuir.6b03606.
9. Artur M. Pinto; Inês C. Gonçalves; A.T. Marques; Graphene-based materials biocompatibility: A review. *Colloids and Surfaces B: Biointerfaces* **2013**, *111*, 188-202, 10.1016/j.colsurfb.2013.05.022.
10. Oscar N. Ruiz; K. A. Shiral Fernando; Baojiang Wang; Nicholas A. Brown; Pengju George Luo; Nicholas D. McNamara; Marlin Vangsness; Ya-Ping Sun; Christopher E. Bunker; Graphene Oxide: A Nonspecific Enhancer of Cellular Growth. *ACS Nano* **2011**, *5*, 8100-8107, 10.1021/nn202699t.
11. Artur T. Dideikin; Alexander Ya. Vul'; Graphene Oxide and Derivatives: The Place in Graphene Family. *Frontiers in Physics* **2019**, *6*, 149, 10.3389/fphy.2018.00149.
12. Singh, D.P.; Herrera, C.E.; Singh, B.; Singh, S.; Singh, R.K.; Kumar, R. Graphene oxide: An efficient material and recent approach for biotechnological and biomedical applications. Mater. Sci. Eng. C 2018, 86, 173–197.
13. Muazim, K.; Hussain, Z. Graphene oxide—A platform towards theranostics. Mater. Sci. Eng. C 2017, 76, 1274–1288.
14. Lebepe, T.C.; Parani, S.; Vuyelwa, N.; Kodama, T.; Oluwafemi, O.S. Cytotoxicity evaluation of Graphene Oxide against Adherent and Suspension cancer cells. Mater. Lett. 2020, 279, 128470.
15. Jingquan Liu; Liang Cui; Dusan Losic; Graphene and graphene oxide as new nanocarriers for drug delivery applications. *Acta Biomaterialia* **2013**, *9*, 9243-9257, 10.1016/j.actbio.2013.08.016.
16. Catriona McCallion; John Burthem; Karen Rees-Unwin; Alexander Golovanov; Alain Pluen; Graphene in therapeutics delivery: Problems, solutions and future opportunities. *European Journal of Pharmaceutics and Biopharmaceutics* **2016**, *104*, 235-250, 10.1016/j.ejpb.2016.04.015.
17. Dembereldorj, U.; Choi, S.Y.; Ganbold, E.O.; Song, N.W.; Kim, D.; Choo, J.; Lee, S.Y.; Kim, S.; Joo, S.W. Gold Nanorod-Assembled PEGylated Graphene-Oxide Nanocomposites for Photothermal Cancer Therapy. Photochem. Photobiol. 2014, 90, 659–666.

18. Khan, M.S.; Pandey, S.; Bhaisare, M.L.; Gedda, G.; Talib, A.; Wu, H.-F. Graphene oxide@gold nanorods for chemo-photothermal treatment and controlled release of doxorubicin in mice Tumor. Colloids Surf. B Biointerfaces 2017, 160, 543–552.
19. Lim, D.-K.; Barhoumi, A.; Wylie, R.G.; Reznor, G.; Langer, R.S.; Kohane, D.S. Enhanced Photothermal Effect of Plasmonic Nanoparticles Coated with Reduced Graphene Oxide. Nano Lett. 2013, 13, 4075–4079.
20. Moon, H.; Kumar, D.; Kim, H.; Sim, C.; Chang, J.-H.; Kim, J.-M.; Kim, H.; Lim, D.-K. Amplified Photoacoustic Performance and Enhanced Photothermal Stability of Reduced Graphene Oxide Coated Gold Nanorods for Sensitive Photoacoustic Imaging. ACS Nano 2015, 9, 2711–2719.
21. Robinson, J.T.; Tabakman, S.M.; Liang, Y.; Wang, H.; Sanchez Casalongue, H.; Vinh, D.; Dai, H. Ultrasmall Reduced Graphene Oxide with High Near-Infrared Absorbance for Photothermal Therapy. J. Am. Chem. Soc. 2011, 133, 6825–6831.
22. Song, J.; Yang, X.; Jacobson, O.; Lin, L.; Huang, P.; Niu, G.; Ma, Q.; Chen, X. Sequential drug release and enhanced photothermal and photoacoustic effect of hybrid reduced graphene oxide-loaded ultrasmall gold nanorod vesicles for cancer therapy. ACS Nano 2015, 9, 9199–9209.
23. Turcheniuk, K.; Dumych, T.; Bilyy, R.; Turcheniuk, V.; Bouckaert, J.; Vovk, V.; Chopyak, V.; Zaitsev, V.; Mariot, P.; Prevarskaya, N.; et al. Plasmonic photothermal cancer therapy with gold nanorods/reduced graphene oxide core/shell nanocomposites. RSC Adv. 2016, 6, 1600–1610.
24. Xu, C.; Yang, D.; Mei, L.; Li, Q.; Zhu, H.; Wang, T. Targeting chemophotothermal therapy of hepatoma by gold nanorods/graphene oxide core/shell nanocomposites. ACS Appl. Mater. Interfaces 2013, 5, 12911–12920.
25. Qiu, X.; You, X.; Chen, X.; Chen, H.; Dhinakar, A.; Liu, S.; Guo, Z.; Wu, J.; Liu, Z. Development of graphene oxide-wrapped gold nanorods as robust nanoplatform for ultrafast near-infrared SERS bioimaging. Int. J. Nanomed. 2017, 12, 4349–4360.
26. Sun, B.; Wu, J.; Cui, S.; Zhu, H.; An, W.; Fu, Q.; Shao, C.; Yao, A.; Chen, B.; Shi, D. In situ synthesis of graphene oxide/gold nanorods theranostic hybrids for efficient tumor computed tomography imaging and photothermal therapy. Nano Res. 2017, 10, 37–48.
27. Zhang, Z.; Shi, J.; Song, Z.; Zhu, X.; Zhu, Y.; Cao, S. A synergistically enhanced photothermal transition effect from mesoporous silica nanoparticles with gold nanorods wrapped in reduced graphene oxide. J. Mater. Sci. 2018, 53, 1810–1823.
28. Arvand, M.; Gholizadeh, T.M. Gold nanorods–graphene oxide nanocomposite incorporated carbon nanotube paste modified glassy carbon electrode for voltammetric determination of indomethacin. Sens. Actuators B 2013, 186, 622–632.
29. Azimzadeh, M.; Rahaie, M.; Nasirizadeh, N.; Ashtari, K.; Naderi-Manesh, H. An electrochemical nanobiosensor for plasma miRNA-155, based on graphene oxide and gold nanorod, for early

detection of breast cancer. Biosens. Bioelectron. 2016, 77, 99–106.

30. Cao, J.-T.; Yang, J.-J.; Zhao, L.-Z.; Wang, Y.-L.; Wang, H.; Liu, Y.-M.; Ma, S.-H. Graphene oxide@gold nanorods-based multiple-assisted electrochemiluminescence signal amplification strategy for sensitive detection of prostate specific antigen. Biosens. Bioelectron. 2018, 99, 92–98.
31. Fu, X.; Chen, L.; Li, J.; Lin, M.; You, H.; Wang, W. Label-free colorimetric sensor for ultrasensitive detection of heparin based on color quenching of gold nanorods by graphene oxide. Biosens. Bioelectron. 2012, 34, 227–231.
32. Han, X.; Fang, X.; Shi, A.; Wang, J.; Zhang, Y. An electrochemical DNA biosensor based on gold nanorods decorated graphene oxide sheets for sensing platform. Anal. Biochem. 2013, 443, 117–123.
33. Jayabal, S.; Viswanathan, P.; Ramaraj, R. Reduced graphene oxide–gold nanorod composite material stabilized in silicate sol–gel matrix for nitric oxide sensor. RSC Adv. 2014, 4, 33541–33548.
34. Tsolekile, N.; Parani, S.; Matoetoe, M.C.; Songca, S.P.; Oluwafemi, O.S. Evolution of ternary I–III–VI QDs: Synthesis, characterization and application. Nano-Struct. Nano-Objects 2017, 12, 46–56.
35. Fard, J.K.; Jafari, S.; Eghbal, M.A. A review of molecular mechanisms involved in toxicity of nanoparticles. Adv. Pharm. Bull. 2015, 5, 447.
36. Frohlich, E. Cellular targets and mechanisms in the cytotoxic action of non-biodegradable engineered nanoparticles. Curr. Drug Metab. 2013, 14, 976–988.
37. Jones, C.F.; Grainger, D.W. In vitro assessments of nanomaterial toxicity. Adv. Drug Deliv. Rev. 2009, 61, 438–456.
38. Moustafa R. K. Ali; Mohammad Aminur Rahman; Yue Wu; Tiegang Han; Xianghong Peng; Megan A. Mackey; Dongsheng Wang; Hyung Ju Shin; Zhuo G. Chen; HaoPeng Xiao; et al.Ronghu WuYan TangDong M. ShinMostafa A. El-Sayed Efficacy, long-term toxicity, and mechanistic studies of gold nanorods photothermal therapy of cancer in xenograft mice. *Proceedings of the National Academy of Sciences* **2017**, *114*, E3110-E3118, 10.1073/pnas.1619302114.
39. Chaofan Hu; Jianhua Rong; Jianghu Cui; Yunhua Yang; Lufeng Yang; Yaling Wang; Yingliang Liu; Fabrication of a graphene oxide–gold nanorod hybrid material by electrostatic self-assembly for surface-enhanced Raman scattering. *Carbon* **2013**, *51*, 255-264, 10.1016/j.carbon.2012.08.051.
40. Cheng Xu; Darong Yang; Lin Mei; Bingan Lu; Libao Chen; Qiuhong Li; Haizhen Zhu; Taihong Wang; Encapsulating Gold Nanoparticles or Nanorods in Graphene Oxide Shells as a Novel Gene Vector. *ACS Applied Materials & Interfaces* **2013**, *5*, 2715-2724, 10.1021/am400212j.

41. Tomasella, P.; Sanfilippo, V.; Bonaccorso, C.; Cucci, L.M.; Consiglio, G.; Nicosia, A.; Mineo, P.G.; Forte, G.; Satriano, C. Theranostic Nanoplatforms of Thiolated Reduced Graphene Oxide Nanosheets and Gold Nanoparticles. Appl. Sci. 2020, 10, 5529.
42. Turcheniuk, K.; Hage, C.-H.; Spadavecchia, J.; Serrano, A.Y.; Larroulet, I.; Pesquera, A.; Zurutuza, A.; Pisfil, M.G.; Héliot, L.; Boukaert, J. Plasmonic photothermal destruction of uropathogenic E. coli with reduced graphene oxide and core/shell nanocomposites of gold nanorods/reduced graphene oxide. J. Mater. Chem. B 2015, 3, 375–386.
43. Duarte De Melo-Diogo; Cleide Pais-Silva; Diana R. Dias; André F. Moreira; Ilídio J. Correia; Strategies to Improve Cancer Photothermal Therapy Mediated by Nanomaterials. *Advanced Healthcare Materials* **2017**, *6*, 1700073, 10.1002/adhm.201700073.
44. Austin, L.A.; Mackey, M.A.; Dreaden, E.C.; El-Sayed, M.A. The optical, photothermal, and facile surface chemical properties of gold and silver nanoparticles in biodiagnostics, therapy, and drug delivery. Arch. Toxicol. 2014, 88, 1391–1417.
45. Choi, J.; Kim, S.Y. Photothermally enhanced photodynamic therapy based on glutathione-responsive pheophorbide a-conjugated gold nanorod formulations for cancer theranostic applications. J. Ind. Eng. Chem. 2020, 85, 66–74.
46. Cong, B. Gold nanorods: Near-infrared plasmonic photothermal conversion and surface coating. J. Mater. Sci. Chem. Eng. 2014, 2, 20.
47. De Freitas, L.; Zanelatto, L.; Mantovani, M.; Silva, P.; Ceccini, R.; Grecco, C.; Moriyama, L.; Kurachi, C.; Martins, V.; Plepis, A. In vivo photothermal tumour ablation using gold nanorods. Laser Phys. 2013, 23, 066003.
48. Khot, M.I.; Andrew, H.; Svavarsdottir, H.S.; Armstrong, G.; Quyn, A.J.; Jayne, D.G. A Review on the Scope of Photothermal Therapy–Based Nanomedicines in Preclinical Models of Colorectal Cancer. Clin. Colorectal Cancer 2019, 18, e200–e209.
49. Rachel S. Riley; Emily S. Day; Gold nanoparticle-mediated photothermal therapy: applications and opportunities for multimodal cancer treatment. *Wiley Interdisciplinary Reviews: Nanomedicine and Nanobiotechnology* **2017**, *9*, e1449, 10.1002/wnan.1449.
50. Varun P. Pattani Ms; James W. Tunnell; Nanoparticle-mediated photothermal therapy: A comparative study of heating for different particle types. *Lasers in Surgery and Medicine* **2012**, *44*, 675-684, 10.1002/lsm.22072.
51. Eun-Kyung Lim; Taekhoon Kim; Soonmyung Paik; Seungjoo Haam; Yong-Min Huh; Kwangyeol Lee; Nanomaterials for Theranostics: Recent Advances and Future Challenges. *Chemical Reviews* **2014**, *115*, 327-394, 10.1021/cr300213b.
52. Jianjian Zhang; Lulu Ning; Jiaguo Huang; Chi Zhang; Kanyi Pu; Activatable molecular agents for cancer theranostics. *Chemical Science* **2020**, *11*, 618-630, 10.1039/c9sc05460j.

53. Zeer Qi; Jun Shi; Beibei Zhu; Jingguo Li; Shaokui Cao; Gold nanorods/graphene oxide nanosheets immobilized by polydopamine for efficient remotely triggered drug delivery. *Journal of Materials Science* **2020**, *55*, 14530-14543, 10.1007/s10853-020-05050-2.

54. Honghong Rao; Xin Xue; Hongqiang Wang; Zhonghua Xue; Gold nanorod etching-based multicolorimetric sensors: strategies and applications. *Journal of Materials Chemistry C* **2019**, *7*, 4610-4621, 10.1039/c9tc00757a.

55. Jeremy T. Robinson; F. Keith Perkins; Eric S. Snow; Zhongqing Wei; Paul E. Sheehan; Reduced Graphene Oxide Molecular Sensors. *Nano Letters* **2008**, *8*, 3137-3140, 10.1021/nl8013007.

56. Mohammad Zaki Ahmad; Sohail Akhter; Ziyaur Rahman; Shabib Akhter; Mohammed Anwar; Neha Mallik; Farhan Jalees Ahmad; Nanometric gold in cancer nanotechnology: current status and future prospect. *Journal of Pharmacy and Pharmacology* **2012**, *65*, 634-651, 10.1111/jphp.12017.

57. Chenming Xue; Chih-Chien Kung; Min Gao; Chung-Chiun Liu; Liming Dai; Augustine M Urbas; Quan Li; Facile fabrication of 3D layer-by-layer graphene-gold nanorod hybrid architecture for hydrogen peroxide based electrochemical biosensor. *Sensing and Bio-Sensing Research* **2015**, *3*, 7-11, 10.1016/j.sbsr.2014.10.008.

58. Deng, K.; Li, C.; Li, X.; Huang, H. Simultaneous detection of sunset yellow and tartrazine using the nanohybrid of gold nanorods decorated graphene oxide. J. Electroanal. Chem. 2016, 780, 296–302.

59. Nirala, N.R.; Abraham, S.; Kumar, V.; Pandey, S.A.; Yadav, U.; Srivastava, M.; Srivastava, S.K.; Singh, V.N.; Kayastha, A.M.; Srivastava, A.; et al. Partially reduced graphene oxide–gold nanorods composite based bioelectrode of improved sensing performance. Talanta 2015, 144, 745–754.

60. Shi, A.; Wang, J.; Han, X.; Fang, X.; Zhang, Y. A sensitive electrochemical DNA biosensor based on gold nanomaterial and graphene amplified signal. Sens. Actuators B 2014, 200, 206–212.

61. Jia Zhang; Ying Sun; Bo Xu; Hua Zhang; Yan Gao; Hanqi Zhang; DaQian Song; A novel surface plasmon resonance biosensor based on graphene oxide decorated with gold nanorod–antibody conjugates for determination of transferrin. *Biosensors and Bioelectronics* **2013**, *45*, 230-236, 10.1016/j.bios.2013.02.008.

62. Saravanan Govindaraju; Kyusik Yun; Synthesis of gold nanomaterials and their cancer-related biomedical applications: an update. *3 Biotech* **2018**, *8*, 113, 10.1007/s13205-018-1137-y.

63. Charles R. Martin; Nanomaterials: A Membrane-Based Synthetic Approach. *Science* **1994**, *266*, 1961-1966, 10.1126/science.266.5193.1961.

64. Minghuan Liu; Chaohui Zheng; Malin Cui; Xiaoyan Zhang; Da-Peng Yang; Xiansong Wang; Daxiang Cui; Graphene oxide wrapped with gold nanorods as a tag in a SERS based

immunoassay for the hepatitis B surface antigen. *Microchimica Acta* **2018**, *185*, 458, 10.1007/s00604-018-2989-x.

65. Yunxiao Li; ZhengPing Li; Weixiang Ye; Shuang Zhao; Qiaochun Yang; Song Ma; Gang Xiao; Guohua Liu; Yong Wang; Zhao Yue; et al. Gold nanorods and graphene oxide enhanced BSA-AgInS2 quantum dot-based photoelectrochemical sensors for detection of dopamine. *Electrochimica Acta* **2019**, *295*, 1006-1016, 10.1016/j.electacta.2018.11.121.